Spurious dipole mode in random-phase approximation and in models based on this approximation

V. Tselyaev [*]

St. Petersburg State University, St. Petersburg 199034, Russia

The problems related to the existence of the spurious dipole mode (SDM) in self-consistent nuclear-structure models are considered. A method is formulated that allows one to eliminate the coupling of the SDM with the physical modes in the extended random-phase approximation (ERPA) theories, in particular, in the time blocking approximation (TBA), which is a model of the ERPA type. It is shown that the application of this method in realistic TBA calculations of the $E1$ excitations gives results which are very close to the results of TBA calculations without using this method if the bare external-field $E1$ operators are replaced by effective ones.

I. INTRODUCTION

The existence of spurious modes (or so-called ghost modes) is a general feature of models based on the concept of the mean field. These modes emerge as a result of the symmetry breaking in the ground state of the quantum many-particle system generated by the mean field, and for this reason they are usually associated with the Nambu-Goldstone modes. The general properties of spurious modes can be deduced within the Green-function method from the consistency relations, see [1–3], which are analogous to the Ward identities known in quantum field theory. The spurious modes should have the zero energy, but in real calculations of the excitation spectra this condition is fulfilled only approximately because of computational limitations.

In nuclear structure theory, the spurious dipole mode (SDM) is a consequence of the breaking of translational symmetry in finite nuclei under the condition that the underlying exact many-body Hamiltonian is translation invariant. The translational symmetry is explicitly broken in the independent-particle model (IPM) in which the dynamics of the nucleus is fully determined by the single-particle Hamiltonian including the mean field. In the IPM, the SDM is mixed with the physical modes and cannot be separated from them. Note that the breaking of translational symmetry in the IPM takes place even if the mean field is self-consistent, in particular if it is determined within the Hartree-Fock approximation [4,5] or within the density functional theory (DFT; see, e.g., Refs. [6–8]).

The mixing of the SDM with the physical modes is the long-standing problem existing in many nuclear-structure models. This problem has been actively discussed in the literature since the 1950s; see, e.g., Refs. [9–11]. A number of methods have been developed to solve it, in particular within approaches aimed at the exact treatment of the nuclear many-body problem (see, e.g., [12–17] and references therein).

The simplest model in which the SDM emerges in an explicit form is the self-consistent random-phase approximation (RPA). In this model the SDM has exactly zero energy and thereby is separated from the physical modes; see [4,5,18]. This fact is usually treated as the restoration of the translational symmetry broken at the IPM level. Nevertheless, in practice, the separation of the SDM from the physical modes in the self-consistent RPA is not complete for two reasons: (i) there is residual mixing of the SDM with the other modes caused by the approximations of the numerical solution of the RPA equations, and (ii) all the modes including the SDM enter the spectral representations of both the exact and the approximate RPA response functions on an equal footing. This in turn leads to two problems: (i) explicit extraction of the SDM terms from the RPA response function and elimination of the residual SDM admixtures from the RPA physical modes, see [19–21], and (ii) elimination of the coupling of the SDM with the physical degrees of freedom in beyond-RPA models in which the RPA response functions (containing the SDM terms) enter as the building blocks; see [22–26]. In the present paper these problems are considered with the use of the methods developed in Refs. [27,28]. The analysis is based on the self-consistent RPA constructed within the DFT.

The paper is organized as follows. In Sec. II, the formalism of the self-consistent RPA is outlined and the properties of the SDM in the RPA are analyzed. In Sec. III, the problem of the SDM in RPA-based models is considered. In particular, the method of elimination of the SDM in extended RPA theories is formulated. Numerical illustrations of these results are presented in Sec. IV. Conclusions are given in the last section.

II. SPURIOUS MODES IN THE SELF-CONSISTENT RPA

A. RPA framework

The RPA is a model which enables one to calculate the energies and the transition amplitudes of the excited states of the quantum many-particle system. It is described in many textbooks; see, e.g., Refs. [4,5]. The main RPA equation can

————
[*]tselyaev@mail.ru

be written in the form

$$\sum_{34} \Omega^{\text{RPA}}_{12,34} z^n_{34} = \omega_n z^n_{12} \tag{1a}$$

or symbolically

$$\Omega^{\text{RPA}} |z^n\rangle = \omega_n |z^n\rangle. \tag{1b}$$

Here and in the following the numerical indices $(1, 2, 3, \ldots)$ stand for the sets of the quantum numbers of some single-particle basis, ω_n is the excitation energy, and z^n_{12} is the transition amplitude. The RPA matrix $\Omega^{\text{RPA}}_{12,34}$ has the form

$$\Omega^{\text{RPA}}_{12,34} = h_{13} \delta_{42} - \delta_{13} h_{42} + \sum_{56} M^{\text{RPA}}_{12,56} V_{56,34}, \tag{2}$$

where h_{12} is the single-particle Hamiltonian, $V_{12,34}$ is the amplitude of the residual interaction, and $M^{\text{RPA}}_{12,34}$ is the metric matrix in the RPA. It is defined as

$$M^{\text{RPA}}_{12,34} = \delta_{13} \rho_{42} - \rho_{13} \delta_{42}, \tag{3}$$

where ρ_{12} is the single-particle density matrix. The matrices ρ and h satisfy the equations

$$\rho^2 = \rho, \quad [h, \rho] = 0, \tag{4}$$

which play the role of the single-particle equations of motion.

It is convenient to introduce the single-particle basis that diagonalizes matrices ρ and h:

$$h_{12} = \varepsilon_1 \delta_{12}, \quad \rho_{12} = n_1 \delta_{12}, \tag{5}$$

where n_1 is the occupation number. In what follows the indices p and h will be used to label the single-particle states of the particles ($n_p = 0$) and holes ($n_h = 1$) in this basis. The matrices $\Omega^{\text{RPA}}_{12,34}$ and $M^{\text{RPA}}_{12,34}$ act in the one-particle–one-hole (1p1h) configuration space. Correspondingly, the transition amplitudes z^n_{12} have only ph and hp components.

In the self-consistent RPA based on the DFT, the single-particle Hamiltonian and the amplitude of the residual interaction are deduced from some energy-density functional (EDF) $E[\rho]$ and are determined by the formulas

$$h_{12} = \frac{\delta E[\rho]}{\delta \rho_{21}}, \quad V_{12,34} = \frac{\delta^2 E[\rho]}{\delta \rho_{21} \delta \rho_{34}}. \tag{6}$$

B. Elimination of the RPA spurious modes in the general case

A conventional tool for the description of nuclear excitations in the quantum many-body theory is the response function formalism. The response function $R(\omega)$ determines the distribution of the strength of transitions in the nucleus caused by some external field represented by the single-particle operator Q according to the formulas

$$S(E) = -\frac{1}{\pi} \operatorname{Im} \Pi(E + i\Delta), \tag{7}$$

$$\Pi(\omega) = -\langle Q|R(\omega)|Q\rangle, \tag{8}$$

where $S(E)$ is the strength function, E is an excitation energy, Δ is a smearing parameter, and $\Pi(\omega)$ is the (dynamic) polarizability. In the RPA, the response function is a matrix in the

1p1h space defined as

$$R^{\text{RPA}}(\omega) = -(\omega - \Omega^{\text{RPA}})^{-1} M^{\text{RPA}}. \tag{9}$$

The spectral representation of the matrix $R^{\text{RPA}}(\omega)$ can be written in the form (see [5,27])

$$R^{\text{RPA}}(\omega) = R^{\text{RPA(phys.)}}(\omega) + R^{\text{RPA(spur.)}}(\omega). \tag{10}$$

Here $R^{\text{RPA(phys.)}}(\omega)$ represents the "physical" part of the function $R^{\text{RPA}}(\omega)$ and has the form

$$R^{\text{RPA(phys.)}}(\omega) = -\sum_n{}' \frac{\operatorname{sgn}(\omega_n)|z^n\rangle\langle z^n|}{\omega - \omega_n}, \tag{11}$$

where ω_n and $|z^n\rangle$ are solutions of Eq. (1b), symbol $\sum'$ means the sum over all the "physical" modes n (that is, the modes with nonzero ω_n) for which the following orthonormalization relation is fulfilled:

$$\langle z^n|M^{\text{RPA}}|z^{n'}\rangle = \operatorname{sgn}(\omega_n)\, \delta_{n,\,n'}. \tag{12}$$

The function $R^{\text{RPA(spur.)}}(\omega)$ represents the "ghost" part of the RPA response function caused by the symmetry breaking. It consists of two terms having poles at $\omega = 0$ corresponding to the spurious modes:

$$R^{\text{RPA(spur.)}}(\omega) = -\frac{a^{(0,1)}}{\omega} - \frac{a^{(0,2)}}{\omega^2}. \tag{13}$$

The matrices $a^{(0,1)}$ and $a^{(0,2)}$ are Hermitian and satisfy the equations (see [27])

$$\Omega^{\text{RPA}} a^{(0,1)} = a^{(0,2)}, \quad \Omega^{\text{RPA}} a^{(0,2)} = 0, \tag{14}$$

$$a^{(0,1)} M^{\text{RPA}} a^{(0,k)} = a^{(0,k)}, \quad k = 1, 2, \tag{15}$$

$$a^{(0,1)} = -\mathfrak{P}\, a^{(0,1)*}\mathfrak{P}, \quad a^{(0,2)} = \mathfrak{P}\, a^{(0,2)*}\mathfrak{P}, \tag{16}$$

where $\mathfrak{P}$ is the permutation operator acting in the space of the pairs of the single-particle indices: $\mathfrak{P}_{12,34} = \delta_{14}\delta_{23}$. In addition, the following closure relation is fulfilled:

$$a^{(0,1)} + \sum_n{}' \operatorname{sgn}(\omega_n)|z^n\rangle\langle z^n| = M^{\text{RPA}}. \tag{17}$$

The properties (15) of the matrices $a^{(0,1)}$ and $a^{(0,2)}$ enable one to introduce a projection operator (see [28]):

$$P = 1 - a^{(0,1)} M^{\text{RPA}}. \tag{18}$$

From Eq. (15) it follows that

$$P^2 = P, \quad P\, a^{(0,1)} = P\, a^{(0,2)} = 0. \tag{19}$$

Equations (12) and (17) yield for the "physical" modes

$$P|z^n\rangle = |z^n\rangle. \tag{20}$$

Thus, from (10), (11), (13), (19), and (20) one obtains

$$P R^{\text{RPA}}(\omega) P^\dagger = R^{\text{RPA(phys.)}}(\omega), \tag{21}$$

that solves the problem of the elimination of the spurious modes in the RPA in the general case if the matrix $a^{(0,1)}$ is known.

Equation (21) can be used in particular if the external field represented by the operator Q can excite the spurious modes. In this case the dynamic polarizability in Eq. (8) is divided

into the "physical" and "ghost" parts analogously to Eq. (10). From Eqs. (21) and (18) it follows that the "physical" part of the RPA polarizability can be extracted by means of the equation

$$\Pi^{\text{RPA(phys.)}}(\omega) = -\langle Q^{\text{eff}} | R^{\text{RPA}}(\omega) | Q^{\text{eff}} \rangle, \qquad (22)$$

where Q^{eff} is the effective external-field operator determined as

$$Q^{\text{eff}} = P^\dagger Q = (1 - M^{\text{RPA}} a^{(0,1)}) Q. \qquad (23)$$

The above equation is analogous to the results of Ref. [20] obtained within the framework of the quasiparticle RPA formalism.

C. The case of the SDM

The explicit form of the matrices $a^{(0,1)}$ and $a^{(0,2)}$ can be found in the important case of the SDM. It is known (see Ref. [4]) that the eigenvectors of this mode are non-normalizable in the sense of Eq. (12). So, it is convenient to proceed in the way described in Ref. [28]. The EDF $E[\rho]$ in Eqs. (6) can be represented as a sum of two terms,

$$E[\rho] = \text{Tr} \, (\rho \, h^0) + E_{\text{int}}[\rho], \qquad (24)$$

where h^0 is a single-particle operator and the term $E_{\text{int}}[\rho]$ contains all contributions to the total energy related to the interaction. Actually, h^0 is a simple kinetic-energy operator but in order to deal in the following with the normalizable solutions of the RPA equations it is convenient to include an oscillator potential into h^0 by setting

$$h^0 = \frac{\mathbf{p}^2}{2m} + \frac{\omega_0^2 m r^2}{2 \hbar^2}, \qquad (25)$$

where $\mathbf{p} = -i\hbar \nabla$ is the momentum operator and m is the nucleon mass (generally different for the neutrons and protons). The functional $E_{\text{int}}[\rho]$ is supposed to be invariant under the symmetry transformations of the type

$$E_{\text{int}}[e^{-i\alpha q} \rho \, e^{i\alpha q}] = E_{\text{int}}[\rho], \qquad (26)$$

where q is a Hermitian single-particle operator and α is an arbitrary real parameter. Differentiation of Eq. (26) with respect to α and ρ with subsequently setting $\alpha = 0$ yields

$$[h, q]_{12} + \sum_{34} V_{12,34} [q, \rho]_{34} = [h^0, q]_{12}, \qquad (27)$$

where Eqs. (6) and (24) were taken into account. Multiplying Eq. (27) from the left with the matrix M^{RPA} and using definitions (2) and (3) and equality $[h, \rho] = 0$, one gets

$$\sum_{34} \Omega_{12,34}^{\text{RPA}} [q, \rho]_{34} = [[h^0, q], \rho]_{12}. \qquad (28)$$

Now, it should be taken into account that the functional $E_{\text{int}}[\rho]$ has to be invariant under translations and Galilean transformations, and that it is a common property of all traditional nuclear EDFs; see [6–8] (notice, however, that in the general case Galilean invariance is compatible with the isotopic symmetry only under the assumption that the masses of neutrons and protons are equal to each other). This means that Eqs. (26)–(28) should be fulfilled for those operators q

which are the space components of the momentum operator ($\mathbf{p}$) and of the coordinate operator multiplied by the nucleon mass ($m\mathbf{r}$). In the case of the operator h^0 defined by Eq. (25) one has

$$[h^0, \nabla] = -\frac{\omega_0^2}{\hbar^2} m\mathbf{r}, \quad [h^0, m\mathbf{r}] = -\hbar^2 \nabla. \qquad (29)$$

From Eqs. (28) and (29), after some algebra one arrives at the following equation:

$$\sum_{34} \Omega_{12,34}^{\text{RPA}} \, \mathbf{z}_{34}^{(\pm)} = \pm \omega_0 \, \mathbf{z}_{12}^{(\pm)}, \qquad (30)$$

where

$$\mathbf{z}_{12}^{(\pm)} = \frac{\hbar}{\sqrt{2\omega_0 M_0}} \left([\nabla, \rho]_{12} \mp \frac{\omega_0}{\hbar^2} [m\mathbf{r}, \rho]_{12} \right), \qquad (31)$$

$M_0 = \text{Tr}(\rho m)$ is the total mass of the nucleus, and it is supposed that $\omega_0 > 0$. The transition amplitudes $\mathbf{z}_{12}^{(\pm)}$ are normalized according to Eq. (12). These amplitudes represent the explicit solutions of the RPA eigenvalue equation (1a) obtained from the symmetry properties of the EDF. They correspond to the spurious 1^- excitations. In Ref. [29], the analogous formulas were obtained for the transition amplitudes of the SDM entering the spectral representation of the exact response function.

If ω_0 is finite, one can substitute the solutions (31) into the right-hand side (r.h.s.) of Eq. (11). In the limit $\omega_0 \to +0$ the contribution of these solutions into the RPA response function takes the form of the r.h.s. of Eq. (13) with

$$a_{12,34}^{(0,1)} = \frac{1}{M_0} ([\nabla, \rho]_{12} \cdot [m\mathbf{r}, \rho]_{43} - [m\mathbf{r}, \rho]_{12} \cdot [\nabla, \rho]_{43}), \qquad (32)$$

$$a_{12,34}^{(0,2)} = \frac{\hbar^2}{M_0} [\nabla, \rho]_{12} \cdot [\nabla, \rho]_{43}. \qquad (33)$$

In the particle-hole (p-h) representation defined by Eqs. (5), the formulas (10), (11), (13), (32), and (33) correspond to Eq. (10.51b) of Ref. [5].

The matrices $a^{(0,1)}$ and $a^{(0,2)}$ defined by Eqs. (32) and (33) are Hermitian. It is not difficult to verify that they satisfy Eqs. (14)–(16). Therefore, the projection operator defined by Eqs. (18) and (32) also satisfies all the conditions described in Sec. II B.

Equations (23) and (32) can be used for determination of the effective external-field operators in the case of the electric dipole excitations. Consider the local vector $E1$ operator Q of the form

$$\mathbf{Q} = f_\tau(r) \mathbf{r}, \qquad (34)$$

where τ is the isotopic index ($\tau = n, p$) and $r = |\mathbf{r}|$. In the following, two kinds of the (bare) radial form factors $f_\tau(r)$ will be considered:

$$f_\tau(r) = \delta_{\tau,p} C_1, \quad C_1 = e \sqrt{3/4\pi}, \qquad (35)$$

in which case $\mathbf{Q}$ in Eq. (34) is the usual electric dipole operator, see [4], and

$$f_\tau(r) = C_0 r^2, \qquad (36)$$

where C_0 is a constant, in which case $\boldsymbol{Q}$ is the isoscalar $E1$ operator. Assuming that the local single-particle density $\rho_\tau(r)$ is spherically symmetric [$\rho_\tau(r) = \sum_s \rho(\boldsymbol{r}, s, \tau; \boldsymbol{r}, s, \tau)$, where s is the spin variable], one obtains from (23), (32), and (34)

$$\boldsymbol{Q}^{\text{eff}} = f_\tau^{\text{eff}}(r)\,\boldsymbol{r}, \qquad (37)$$

where

$$f_\tau^{\text{eff}}(r) = f_\tau(r) - \frac{m_\tau}{M_0}\bar{f}, \qquad (38)$$

$$\bar{f} = \sum_\tau \int d\boldsymbol{r}\,\rho_\tau(r)\Big[f_\tau(r) + \frac{r}{3}f_\tau'(r)\Big]. \qquad (39)$$

In the case of the form factor (35), Eqs. (38) and (39) yield

$$f_p^{\text{eff}}(r) = \tilde{C}_1 N/A, \quad f_n^{\text{eff}}(r) = -\tilde{C}_1 Z/A, \qquad (40)$$

where $\tilde{C}_1 = C_1 A m_n/M_0$, $A = N + Z$, and $M_0 = N m_n + Z m_p$; N and Z are the numbers of neutrons and protons, respectively. If in addition the equality $m_n = m_p$ is assumed, Eqs. (37) and (40) correspond to the known formulas for the effective nucleon $E1$ charges; see [4].

In the case of the form factor (36), assuming again the equality $m_n = m_p$, one obtains from Eqs. (38) and (39)

$$f_\tau^{\text{eff}}(r) = C_0\big(r^2 - \tfrac{5}{3}\langle r^2\rangle\big), \qquad (41)$$

where $\langle r^2\rangle = \text{Tr}(\rho r^2)/A$, that also corresponds to the known formula [30] for this case.

Further, from Eq. (12) it follows that the spurious amplitudes (31) at finite ω_0 are orthogonal to the "physical" ones $|z^n\rangle$, that is

$$\langle z^n|M^{\text{RPA}}|\boldsymbol{z}^{(\pm)}\rangle = 0. \qquad (42)$$

Using this equality and the definitions (3) and (31) one obtains

$$\langle z^n|m\boldsymbol{r}\rangle = 0, \quad \langle z^n|\nabla\rangle = 0. \qquad (43)$$

Obviously, Eqs. (43) remain valid in the limit $\omega_0 \to +0$. From Eqs. (32) and (33) one also has

$$a^{(0,1)}|m\boldsymbol{r}\rangle = |[m\boldsymbol{r}, \rho]\rangle, \qquad (44)$$

$$a^{(0,2)}|m\boldsymbol{r}\rangle = -\hbar^2|[\nabla, \rho]\rangle, \qquad (45)$$

$$a^{(0,1)}|\nabla\rangle = |[\nabla, \rho]\rangle, \qquad (46)$$

$$a^{(0,2)}|\nabla\rangle = 0. \qquad (47)$$

Note that, in the derivation considered above, only the symmetry properties of the EDF $E[\rho]$ entering the RPA equations (1)–(6) were used. The symmetry properties of the underlying *exact* many-body Hamiltonian (which includes bare internucleon interactions) were not taken into account explicitly, though in fact they determine the properties of the EDF. However, this exact Hamiltonian is not immediately connected with real EDFs used in the RPA calculations. In practice, the nuclear EDFs are frequently derived from the Hartree-Fock expectation values of the certain *effective* many-body Hamiltonians, and the symmetry properties of these Hamiltonians may differ from the properties of the exact Hamiltonian. In particular, the effective Hamiltonian is not translation invariant if it includes the density-dependent effective interactions, e.g., interactions of the Skyrme type.

Moreover, the EDF can be constructed formally without reference to any many-body Hamiltonian; see Ref. [6] for discussion of this point. For all these reasons, the EDF-based analysis of the spurious modes is more adequate for the framework of the self-consistent RPA as compared to the analysis based on the properties of the many-body Hamiltonians.

Note also that the energy of the SDM can be shifted to zero even in the non-self-consistent RPA by introducing the additional terms of the separable form in the residual interaction (see Refs. [31,32] and references in [32] for recent applications of this method). In the self-consistent RPA, these additional terms are unnecessary because the zero energy of the SDM is guaranteed by the fulfillment of Eq. (30) at $\omega_0 \to +0$, which is a consequence of the relation between the mean field and the residual interaction determined by Eqs. (6) and of the symmetry conditions (26).

III. SDM IN RPA-BASED MODELS

A. RPA treatment of core-polarization effects in even-odd nuclei and the SDM

Consider the problem of describing the transition probabilities for the states of even-odd nuclei supposing that these states are single-particle ones and that the transitions between them are caused by the external field represented by the single-particle operator Q. In this case the transition probabilities are determined by the matrix elements $\tilde{Q}_{12}$ of the effective operator $\tilde{Q}$ which is the sum of the bare operator Q and the core-polarization term ΔQ:

$$\tilde{Q}_{12} = Q_{12} + \Delta Q_{12}. \qquad (48)$$

The treatment of the term ΔQ within the RPA was developed and described in Refs. [2,33,34] (see also discussion of this treatment in [35]). It can be represented in the form

$$\Delta Q_{12} = -\sum_{3456} V_{12,34}\,R^{\text{RPA}}_{34,56}(\varepsilon_{12})\,Q_{56}, \qquad (49)$$

where the RPA response function $R^{\text{RPA}}(\omega)$ is defined in Eq. (9), and $\varepsilon_{12} = \varepsilon_1 - \varepsilon_2$ with ε_1 determined by Eq. (5).

If the external field is represented by the operators $\boldsymbol{Q} = m\boldsymbol{r}$ or $\boldsymbol{Q} = \nabla$, it acts only on the center-of-mass coordinate and thus should not give rise to the transitions between the intrinsic states of the nucleus. So, in this case the effective operator $\tilde{\boldsymbol{Q}}$ should be equal to zero.

As follows from the results of Sec. II C, in the self-consistent RPA from Eqs. (11) and (43) one has

$$R^{\text{RPA(phys.)}}(\omega)|m\boldsymbol{r}\rangle = R^{\text{RPA(phys.)}}(\omega)|\nabla\rangle = 0. \qquad (50)$$

On the other hand, from Eqs. (5), (13), (27), (29), and (44)–(47) it follows that

$$\sum_{3456} V_{12,34}\,R^{\text{RPA(spur.)}}_{34,56}(\varepsilon_{12})\,(m\boldsymbol{r})_{56} = (m\boldsymbol{r})_{12}, \qquad (51)$$

$$\sum_{3456} V_{12,34}\,R^{\text{RPA(spur.)}}_{34,56}(\varepsilon_{12})\,\nabla_{56} = \nabla_{12}. \qquad (52)$$

Therefore, from Eqs. (10) and (48)–(52) one obtains that $\tilde{\boldsymbol{Q}} = 0$ for the external-field operators $\boldsymbol{Q} = m\boldsymbol{r}$ and $\boldsymbol{Q} = \nabla$ if the quantities V, $R^{\text{RPA}}(\omega)$, and ε_{12} in (49) are determined in

the self-consistent RPA and if the contribution of the SDM is included in the $R^{\mathrm{RPA}}(\omega)$.

B. Elimination of the SDM in extended RPA theories

It is well known that in the general case the response function can be defined as a solution of the Bethe-Salpeter equation (BSE; see, e.g., Ref. [2]). In the case of the RPA response function defined by Eq. (9), the BSE reads

$$R^{\mathrm{RPA}}(\omega) = R^{(0)}(\omega) - R^{(0)}(\omega) V R^{\mathrm{RPA}}(\omega), \qquad (53)$$

where $R^{(0)}(\omega)$ is uncorrelated p-h propagator and V is the amplitude of the residual interaction entering the RPA matrix (2). All the matrices in Eq. (53) are defined in the 1p1h configuration space. The p-h propagator $R^{(0)}(\omega)$ is defined as

$$R^{(0)}(\omega) = -(\omega - \Omega^{(0)})^{-1} M^{\mathrm{RPA}}, \qquad (54)$$

where

$$\Omega^{(0)}_{12,34} = h_{13}\,\delta_{42} - \delta_{13}\,h_{42} \qquad (55)$$

and M^{RPA} is the metric matrix (3).

In the beyond-RPA models, the 1p1h configuration space of the RPA is extended by including more complex configurations, e.g., of the 2p2h, 1p1h $\otimes$ phonon, or two-phonon type, where the phonons in the simplest case are superpositions of the 1p1h configurations represented by the solutions of the RPA equation (1). In the following, extended RPA (ERPA) theories are considered in which the response function is determined by the BSE of the form

$$R^{\mathrm{ERPA}}(\omega) = R^{(0)}(\omega) - R^{(0)}(\omega)\,[V + \bar{W}(\omega)]\,R^{\mathrm{ERPA}}(\omega), \qquad (56)$$

which can be also rewritten as

$$R^{\mathrm{ERPA}}(\omega) = R^{\mathrm{RPA}}(\omega) - R^{\mathrm{RPA}}(\omega)\bar{W}(\omega)R^{\mathrm{ERPA}}(\omega). \qquad (57)$$

Here $\bar{W}(\omega)$ is the (subtracted) amplitude of the induced interaction including contributions of complex configurations. This amplitude is the energy-dependent matrix in the 1p1h space. It has the form

$$\bar{W}_{12,34}(\omega) = W_{12,34}(\omega) - W_{12,34}(0) \qquad (58)$$

with

$$W_{12,34}(\omega) = \sum_{c,\,\sigma} \frac{\sigma\, F^{c(\sigma)}_{12} F^{c(\sigma)*}_{34}}{\omega - \sigma\,\Omega_c}, \qquad (59)$$

where $\sigma = \pm 1$ and c is an index of the subspace of complex configurations. Explicit formulas for the amplitudes $F^{c(\sigma)}_{12}$ and the energies Ω_c in the case of some models of the ERPA type are given in Ref. [27]. Note that in the models considered in [27] all the energies of complex configurations Ω_c are positive.

The subtraction of the amplitude $W(0)$ in Eq. (58) ensures the stability of solutions of the ERPA equations (see [27] for more details). At present, this subtraction method is used in beyond-RPA models including 1p1h $\otimes$ phonon [36–41] and 2p2h [42,43] configurations. As follows from Eq. (57), the subtraction of $W(0)$ also ensures the existence of the poles of $R^{\mathrm{ERPA}}(\omega)$ at $\omega = 0$ if these poles (corresponding to the spurious modes) exist in the RPA response function determined

by Eq. (53). This property was one of the motivations for introducing this method in Ref. [44]. However, the subtraction method in itself does not exclude the residual coupling of the spurious modes with the physical ones mediated by the amplitude $\bar{W}(\omega)$ at nonzero energies. As a result, though the main component of the spurious state appears at zero energy, its fragments can be spread out over a wide energy range.

Formally, the contribution of the spurious states is completely absent in the response function $R^{\mathrm{ERPA(phys.)}}(\omega)$ defined by the equation

$$\begin{aligned} R^{\mathrm{ERPA(phys.)}}(\omega) &= R^{\mathrm{RPA(phys.)}}(\omega) \\ &\quad - R^{\mathrm{RPA(phys.)}}(\omega)\bar{W}(\omega)R^{\mathrm{ERPA(phys.)}}(\omega), \end{aligned} \qquad (60)$$

where the function $R^{\mathrm{RPA(phys.)}}(\omega)$ is formally determined by Eq. (11). In the case of the SDM in the self-consistent RPA, the function $R^{\mathrm{RPA(phys.)}}(\omega)$ can be determined in practice by Eqs. (21), (18), and (32). However, such determination of $R^{\mathrm{ERPA(phys.)}}(\omega)$ requires first solving the RPA BSE (53), which complicates the task.

A more convenient method for the elimination of the SDM in the ERPA was suggested in Ref. [28]. Consider a function $R^{\mathrm{ERPA+}}(\omega)$ which is a solution of the equation

$$R^{\mathrm{ERPA+}}(\omega) = R^{(0)}(\omega) - R^{(0)}(\omega)\,[V + \bar{W}^{\perp}(\omega)]\,R^{\mathrm{ERPA+}}(\omega), \qquad (61)$$

where the amplitude $\bar{W}^{\perp}(\omega)$ is defined as

$$\bar{W}^{\perp}(\omega) = P^{\dagger}\bar{W}(\omega)P \qquad (62)$$

with the operator P defined in Eqs. (18) and (32). In fact, Eq. (61) is analogous to Eq. (56) and is equivalent to Eq. (57) in which the amplitude $\bar{W}(\omega)$ is replaced by $\bar{W}^{\perp}(\omega)$. But, as follows from Eqs. (13) and (19), the amplitude $\bar{W}^{\perp}(\omega)$ is orthogonal to the "ghost" part of the RPA response function, because

$$P R^{\mathrm{RPA(spur.)}}(\omega) = R^{\mathrm{RPA(spur.)}}(\omega)P^{\dagger} = 0. \qquad (63)$$

So, the coupling of the spurious modes with the physical ones in Eq. (61) is eliminated.

After a series of transformations, one can show that the solution of Eq. (61) satisfies the equality

$$R^{\mathrm{ERPA+}}(\omega) = R^{\mathrm{ERPA(phys.)}}(\omega) + R^{\mathrm{RPA(spur.)}}(\omega), \qquad (64)$$

where $R^{\mathrm{ERPA(phys.)}}(\omega)$ and $R^{\mathrm{RPA(spur.)}}(\omega)$ are defined by Eqs. (60), (13), (32), and (33). Equation (64) explicitly shows that the SDM is fully separated from the physical modes in the response function $R^{\mathrm{ERPA+}}(\omega)$. At the same time, this function is determined by only one equation, (61), which is the main equation of the given method. In what follows the model corresponding to this equation will be referred to as the ERPA with projection (ERPA+).

The problem of extracting the "physical" part of the RPA response function in a beyond mean-field model was considered in Ref. [26]. Within the formalism described above, the method of Ref. [26] corresponds to introducing the corrected RPA response function $\tilde{R}^{\mathrm{RPA}}(\omega) = \tilde{P}R^{\mathrm{RPA}}(\omega)$,

where

$$\tilde{P} = 1 - \tilde{a}^{(0,1)} M^{\text{RPA}}, \tag{65}$$

$$\tilde{a}^{(0,1)}_{12,34} = \frac{1}{M_0} [\nabla, \rho]_{12} \cdot [m\boldsymbol{r}, \rho]_{43}. \tag{66}$$

Comparing Eqs. (65) and (66) with Eqs. (18) and (32) for the operator P, one can see that

$$P = \tilde{P} - \tilde{a}^{(0,1)\dagger} M^{\text{RPA}}. \tag{67}$$

The absence of the last term of Eq. (67) in the operator $\tilde{P}$ leads to the incomplete elimination of the "ghost" part of $R^{\text{RPA}}(\omega)$ in this method. Indeed, from Eqs. (13), (32), (33), (65), and (66) it follows that

$$\tilde{P} R^{\text{RPA(spur.)}}(\omega) = -\frac{\tilde{a}^{(0,1)\dagger}}{\omega}. \tag{68}$$

The remainder determined by the r.h.s. of Eq. (68) does not contribute to the strength function defined by Eqs. (7) and (8) in the case of the local external-field operators Q considered in [26]. However, the contribution of this remainder can be nonzero in the other cases arising in beyond mean-field models.

IV. NUMERICAL RESULTS

In this section the results of the fully self-consistent calculations of the electric dipole ($E1$) excitations performed in the models based on the Skyrme EDF are presented. Two main models are considered: RPA and the time blocking approximation (TBA), which is a model of the ERPA type including 1p1h $\otimes$ phonon configurations on top of the 1p1h configuration space of the RPA. The general scheme of the TBA is described by Eqs. (56), (58), and (59) of Sec. III B. The detailed formulas of the self-consistent version of this model are given in Refs. [38,39]. Numerical details of the calculations are the following. The RPA and TBA equations were solved in the representation of the discrete p-h basis obtained from the solution of the Skyrme-Hartree-Fock equations (4) and (6) with the box boundary condition. The basis included all the hole states and all the particle states of the single-particle spectrum with energies $\varepsilon_p < \varepsilon_{\text{max}}$. In what follows two versions of the RPA and TBA are used. In the discrete versions (DRPA and DTBA) the effect of the single-particle continuum is not included. In the continuum versions (CRPA and CTBA) this effect is included in the discrete basis representation according to the method described in [39].

A. SDM results in the RPA

In the calculations of the $E1$ excitations within the self-consistent RPA and RPA-based models, the deviation of the SDM energy (ω_{SDM}) from zero can serve as a criterion of accuracy of the calculation scheme. The rigorous equality $\omega_{\text{SDM}} = 0$ implies full self-consistency, that is, exact fulfillment of Eqs. (4) and (6); however, the value of ω_{SDM} strongly depends also on the numerical details, in particular on the size of the p-h basis determined by the parameter ε_{max}. In Fig. 1, the dependence of ω_{SDM} on the value of ε_{max} is shown. The
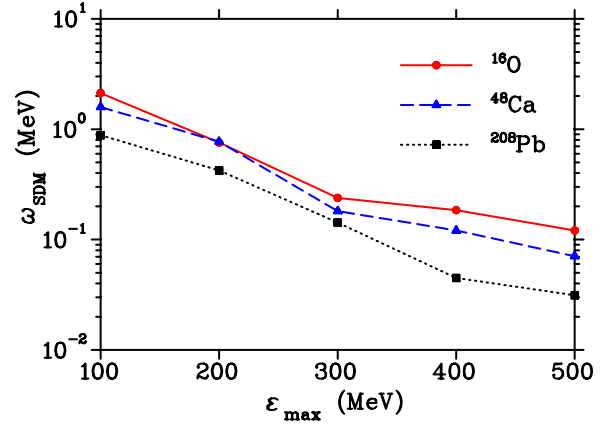
FIG. 1. Dependence of the energy of the spurious dipole mode, ω_{SDM}, on the maximum energy of the states of the single-particle spectrum, ε_{max}. Calculations within the fully self-consistent DRPA based on the Skyrme-EDF parametrization SLy4 for ^{16}O, ^{48}Ca, and ^{208}Pb.

results were obtained in the DRPA for three doubly magic nuclei: ^{16}O, ^{48}Ca, and ^{208}Pb. The Skyrme-EDF parametrization SLy4 [45] was used. The box radius was taken to be 15 fm for ^{16}O and ^{48}Ca and 18 fm for ^{208}Pb. At the increase of ε_{max} from 100 to 500 MeV, the value of ω_{SDM} decreases from 2.13 to 0.12 MeV in ^{16}O, from 1.59 to 0.07 MeV in ^{48}Ca, and from 0.88 to 0.03 MeV in ^{208}Pb. The decrease of ω_{SDM} is monotonic and almost exponential at $\varepsilon_{\text{max}} < 300$ MeV, but is slowed down at greater ε_{max}. In particular, $\omega_{\text{SDM}} \approx 3$ keV in ^{16}O at $\varepsilon_{\text{max}} = 2000$ MeV.

The separation of the SDM from the physical modes can be estimated with the help of the ratio of the reduced probability of the $E1$ transition for the SDM, $B(E1)_{\text{SDM}}$, to the reduced probability $B(E1)_{\text{max}}$ for the DRPA state having the largest $B(E1)$ in the given strength distribution. For the effective $E1$ operator defined by Eqs. (37) and (40), the limiting value of $B(E1)_{\text{SDM}}$ is equal to zero. The calculated values of $B(E1)_{\text{SDM}}/B(E1)_{\text{max}} \lesssim 1.5 \times 10^{-5}$ in the case of $\varepsilon_{\text{max}} = 100$ MeV and $\lesssim 3.3 \times 10^{-9}$ in the case of $\varepsilon_{\text{max}} = 500$ MeV for all three nuclei under consideration. Thus, a fairly good separation of the SDM is achieved in the DRPA already at $\varepsilon_{\text{max}} = 100$ MeV.

B. Center-of-mass motion in the response function formalism

In the ERPA theories, separation of the SDM is attained with the help of the method described in Sec. III B. Consider its implementation in the TBA. The efficiency of this method can be estimated by comparing the calculated response of the nucleus to the external field represented by the operator of the center-of-mass coordinate (c.m.c.),

$$\boldsymbol{Q} = \frac{m}{M_0} \boldsymbol{r}, \tag{69}$$

with the known exact result.

From Eqs. (8), (10), (11), (13), (43)–(45) it follows that the polarizability $\Pi(\omega)$ corresponding to the operator (69) in the
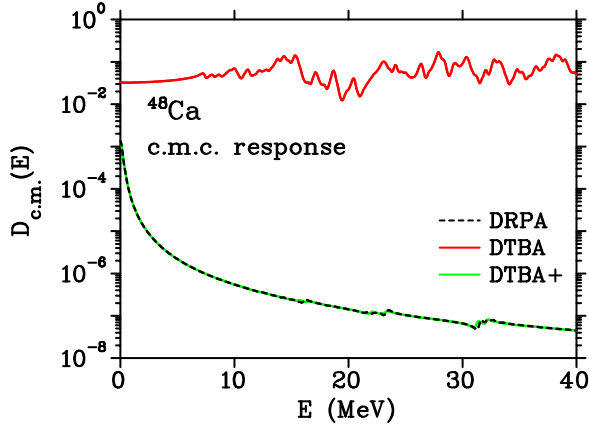
FIG. 2. Energy dependence of the function $D_{c.m.}(E)$, Eq. (71), as the measure of deviation of the calculated polarizability from the exact formula (70) for the response of the nucleus to the external field represented by the operator of the center-of-mass coordinate (c.m.c.). Calculations for ^{48}Ca are shown for the following fully self-consistent models: DRPA (black dashed line), DTBA (red full line), and DTBA+ (green full line) based on the Skyrme-EDF parametrization SLy4. The smearing parameter $\Delta = 200$ keV was used.

self-consistent RPA is equal to

$$\Pi_{c.m.}(\omega) = \frac{3\hbar^2}{M_0\omega^2}. \qquad (70)$$

As follows from Eqs. (60), (61), and (64), the same result for the polarizability is obtained in the self-consistent ERPA+ described in Sec. III B; that is, in the case of the response function $R(\omega) = R^{\text{ERPA+}}(\omega)$ in Eq. (8). On the other hand, in the ERPA without projection the c.m.c. polarizability does not coincide with Eq. (70) in the general case. However, the result expressed by Eq. (70) is not exactly achieved even in the self-consistent RPA and ERPA+ calculations because of the numerical limitations and inaccuracies. The measure of deviation from this exact expression can be determined with the help of the function

$$D_{c.m.}(E) = |\Pi(E + i\Delta)/\Pi_{c.m.}(E + i\Delta) - 1|, \qquad (71)$$

where $\Pi(\omega)$ is the calculated polarizability, E is the real energy variable, and Δ is the smearing parameter.

In Fig. 2, the calculated dependencies $D_{c.m.}(E)$ for the nucleus ^{48}Ca are shown for three fully self-consistent models: DRPA (black dashed line), DTBA (red full line), and DTBA+ (green full line) based on the Skyrme-EDF parametrization SLy4. The p-h basis included all single-particle states up to the energy $\varepsilon_{\max} = 1000$ MeV, which gives $\omega_{\text{SDM}} = 7$ keV. The phonon basis in the DTBA and DTBA+ included three low-lying most collective RPA states with $L^\pi = 2^+$, 3^-, and 5^-, having energies equal to 3.37, 5.61, and 6.03 MeV, respectively. In the calculations of $D_{c.m.}(E)$, the smearing parameter $\Delta = 200$ keV was used. The DRPA and DTBA+ results practically coincide with each other, which demonstrates well performance of the projection method used in the DTBA+. The maximum value of $D_{c.m.}(E)$ in both these models is attained at $E = 0$ and is about $10^{-3} \approx \omega_{\text{SDM}}^2/\Delta^2$. At the large values of E, the function $D_{c.m.}(E) \approx \omega_{\text{SDM}}^2/E^2$ and becomes

less than 10^{-6} at $E > 10$ MeV. This dependence of $D_{c.m.}(E)$ is well approximated by the function

$$\tilde{D}_{c.m.}(E) = \frac{\omega_{\text{SDM}}^2}{\sqrt{(E^2 - \omega_{\text{SDM}}^2 - \Delta^2)^2 + 4E^2\Delta^2}}, \qquad (72)$$

which is obtained from the definitions (69)–(71) and from Eqs. (8), (11), and (31) at finite $\omega_0 = \omega_{\text{SDM}}$. Thus, the degree of separation of the SDM in the ERPA+ calculations is determined by the proximity of ω_{SDM} to zero.

In the DTBA without projection [but with subtraction according to Eq. (58)], the values of $D_{c.m.}(E)$ oscillate within the range from 0.01 up to 0.17 in the considered energy interval, which shows the existing residual coupling of the SDM with the physical modes in this model.

C. Elimination of the SDM in realistic TBA calculations

In this subsection, application of the method of the elimination of the SDM in realistic calculations of $E1$ excitations is considered. The calculations were performed in the nuclei ^{48}Ca, ^{48}Ni, and ^{208}Pb within the renormalized version of the TBA (RenTBA) developed in Ref. [46]. The final equations of both the RenTBA and the TBA have the form of Eqs. (56), (58), and (59) of Sec. III B, but the phonon space in the RenTBA is determined by the system of nonlinear equations. The details of its solution are described in [46] and here are the same as in Ref. [47] except for the space of the phonon renormalization, which in the present paper is common for phonons of electric and magnetic types.

1. E1 excitations in ^{48}Ca and ^{48}Ni

In the calculations of giant resonances in the light nuclei and especially in the light exotic nuclei, the contribution of the single-particle continuum is large. For this reason, it was included in the calculations for ^{48}Ca and proton-rich ^{48}Ni. The abbreviations CTBA and CTBA+ refer here to the RenTBA results. The details of the calculation scheme are the following. The Skyrme-EDF parametrization SV-m64k6 was used. This parametrization was suggested in Ref. [48] (where it was denoted as SV-m64-O) for the description of giant dipole resonances (GDR) in light nuclei. To avoid the spin instability of the ground state, the so-called spin surface terms of the EDF have been omitted (see Ref. [49] for more details). It corresponds to the option $\eta_{\Delta s} = 0$ in terms of Ref. [49]. The p-h basis was restricted by the parameter $\varepsilon_{\max} = 100$ MeV. The box radius was equal to 15 fm in ^{48}Ca and 18 fm in ^{48}Ni. It gives $\omega_{\text{SDM}} = 1.58$ MeV in ^{48}Ca and 1.53 MeV in ^{48}Ni. The resulting phonon space of the RenTBA in ^{48}Ca included eight phonons of electric type with multipolarities $2 \leqslant L \leqslant 6$ and eight phonons of magnetic type with multipolarities $1 \leqslant L \leqslant 5$. The phonon space in ^{48}Ni included fourteen phonons of electric type with multipolarities $2 \leqslant L \leqslant 6$ and seven phonons of magnetic type with multipolarities $2 \leqslant L \leqslant 5$. All the obtained phonons' energies are less than 12 MeV.

In general, the numerical scheme described above is conventional for most TBA and RenTBA calculations. Nevertheless, consider the influence of some elements of this scheme on the results in the case of isoscalar (IS) $E1$
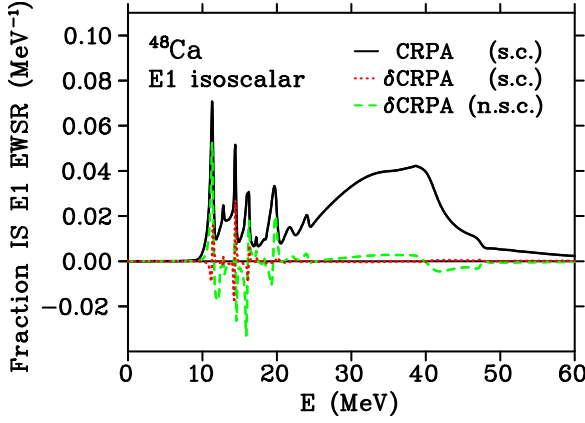
FIG. 3. Strength distribution of the IS $E1$ resonance in ^{48}Ca calculated within the CRPA based on the Skyrme-EDF parametrization SV-m64k6. The black full line corresponds to the fully self-consistent CRPA with $\varepsilon_{\mathrm{max}} = 100$ MeV. The red dotted line represents the difference between the results obtained in fully self-consistent CRPA with $\varepsilon_{\mathrm{max}} = 100$ MeV and $\varepsilon_{\mathrm{max}} = 1000$ MeV. The green dashed line represents the difference between the results obtained in fully self-consistent and non-self-consistent CRPA with $\varepsilon_{\mathrm{max}} = 100$ MeV. The smearing parameter $\Delta = 100$ keV was used. See text for more details.

excitations. Dependence of the SDM energy on the parameter $\varepsilon_{\mathrm{max}}$ was analyzed in Sec. IV A. Dependence of the strength distributions of giant IS $E1$ resonances on this parameter is much less pronounced. Figure 3 shows such a distribution in ^{48}Ca calculated in the CRPA in terms of the fraction of the IS $E1$ energy-weighted sum rule (IS $E1$ EWSR) determined by the function

$$F(E) = E \, S(E)/m_1^{\mathrm{RPA}}, \tag{73}$$

where $S(E)$ is the strength function (7), and

$$m_1^{\mathrm{RPA}} = \int_0^\infty E \, S^{\mathrm{RPA}}(E) \, dE \tag{74}$$

is the first moment of the RPA strength function $S^{\mathrm{RPA}}(E)$.

The function $S(E)$ was calculated for the effective IS $E1$ operator determined by Eqs. (37) and (41). For this operator, the analytic formula for m_1^{RPA} is known (RPA EWSR; see Ref. [30]). The black full line in Fig. 3 represents the function $F_{100}^{\mathrm{s.c.}}(E)$ calculated according to Eq. (73) within the fully self-consistent CRPA with $\varepsilon_{\mathrm{max}} = 100$ MeV and the smearing parameter $\Delta = 100$ keV. The analogous function $F_{1000}^{\mathrm{s.c.}}(E)$ was calculated with $\varepsilon_{\mathrm{max}} = 1000$ MeV (note that $\omega_{\mathrm{SDM}} = 11$ keV for this value of $\varepsilon_{\mathrm{max}}$). The curves corresponding to $F_{100}^{\mathrm{s.c.}}(E)$ and $F_{1000}^{\mathrm{s.c.}}(E)$ are hardly distinguishable from each other in the given scale, so only the difference

$$\delta F^{\mathrm{s.c.}}(E) = F_{100}^{\mathrm{s.c.}}(E) - F_{1000}^{\mathrm{s.c.}}(E), \tag{75}$$

denoted as δCRPA (s.c.), is shown in Fig. 3 by the red dotted line. This difference is not negligible only for three narrow peaks in the region of 11–16.2 MeV which are shifted down in the function $F_{1000}^{\mathrm{s.c.}}(E)$ by the value δE from 30 to 130 keV. The difference $\delta F^{\mathrm{s.c.}}(E)$ practically vanishes in the region of the giant IS $E1$ resonance at $E > 20$ MeV.
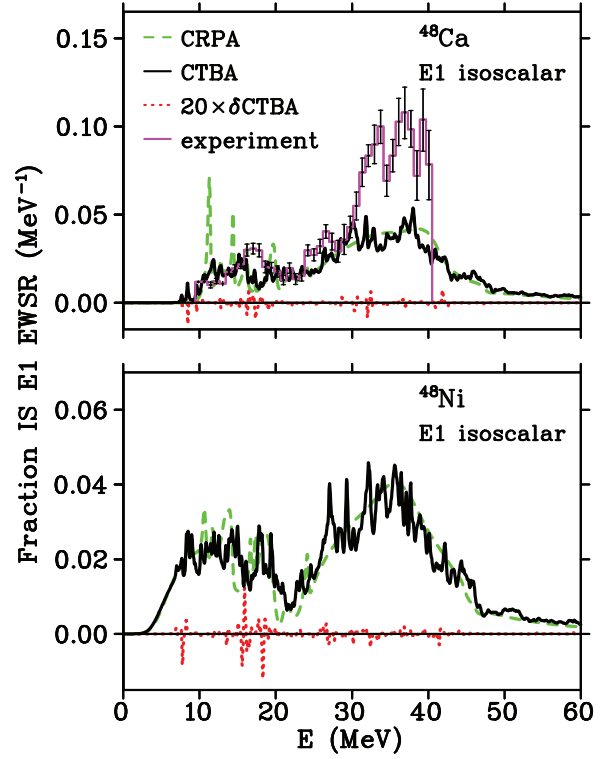
FIG. 4. Upper panel: strength distributions of the isoscalar $E1$ excitations in ^{48}Ca calculated within the CRPA (green dashed line) and CTBA (black full line) based on the Skyrme-EDF parametrization SV-m64k6. The red dotted line represents the difference δCTBA between the CTBA+ and CTBA results multiplied by the factor of 20. The smearing parameter $\Delta = 100$ keV was used. Experimental data (magenta full line with error bars) are taken from Ref. [50]. Lower panel: same as in the upper panel but for ^{48}Ni.

For comparison, the function $F_{100}^{\mathrm{n.s.c.}}(E)$ for the IS $E1$ excitations in ^{48}Ca was calculated by the formula (73) within non-self-consistent CRPA with $\varepsilon_{\mathrm{max}} = 100$ MeV. In this calculation the spin-orbit and Coulomb contributions to the residual interaction V in Eq. (2) have been omitted, which leads to the increase of ω_{SDM} from 1.58 to 2.74 MeV. The difference

$$\delta F^{\mathrm{n.s.c.}}(E) = F_{100}^{\mathrm{s.c.}}(E) - F_{100}^{\mathrm{n.s.c.}}(E) \tag{76}$$

is shown in Fig. 3 by the green dashed line denoted as δCRPA (n.s.c.). As can be seen, this difference does not vanish in the wide region from 10 to 50 MeV.

The results of the CTBA calculations of the IS $E1$ excitations in ^{48}Ca and ^{48}Ni are shown in Fig. 4. They are presented in terms of the fractions of the RPA EWSR determined by Eq. (73). The strength functions in Eq. (73) were calculated with the same smearing parameter $\Delta = 100$ keV as in Fig. 3. The narrow peaks of the CRPA strength distribution in ^{48}Ca in the region below 20 MeV are strongly fragmented in the CTBA, in agreement with the experimental data for this nucleus from Ref. [50]. However, the theory does not describe the large increase of IS $E1$ strength above 30 MeV found experimentally. This discrepancy takes place also in the other
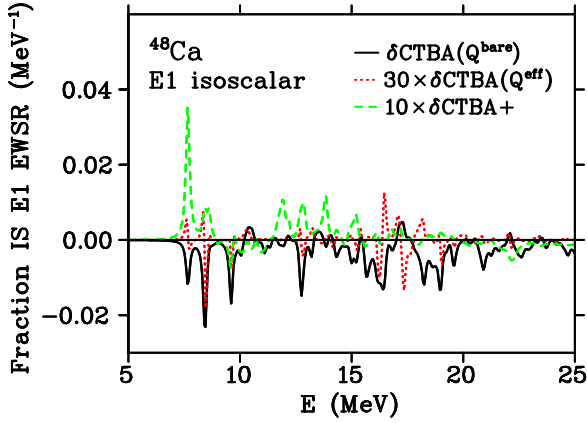
FIG. 5. Differences of the strength distributions of the IS $E1$ resonance in ^{48}Ca calculated within the CTBA based on the Skyrme-EDF parametrization SV-m64k6. The black full line corresponds to the difference δCTBA between the CTBA+ and CTBA results obtained for the bare IS $E1$ operator, (34) and (36). The red dotted line represents the analogous difference for the effective IS $E1$ operator, (37) and (41), multiplied by the factor of 30. The green dashed line represents the difference δCTBA+ between the CTBA+ results obtained for the bare and effective IS $E1$ operators multiplied by the factor of 10. The smearing parameter $\Delta = 100$ keV was used.

RPA calculations of the IS $E1$ giant resonance in ^{48}Ca; see Ref. [51].

The effect of the elimination of the SDM in the CTBA+ can be estimated with the help of the difference (denoted as δCTBA in Fig. 4) between the functions $F(E)$ calculated within the CTBA+ and CTBA. As can be seen from Fig. 4, the relative difference is very small in both nuclei and only scaled δCTBA (multiplied by the factor of 20) is visible. This difference is much less than the differences between the CRPA distributions shown in Fig. 3 and between the DTBA+ and DTBA results for the c.m.c. response shown in Fig. 2. The latter fact needs an explanation.

It should be specified that the results shown in Fig. 4 were obtained for the effective IS $E1$ operator determined by Eqs. (37) and (41). But this operator itself suppresses the spurious admixtures in the excited states as follows from its general definition (23). For this reason, the effect of the projection method used in the CTBA+ is better seen in the calculations of the IS $E1$ response for the bare operator determined by Eqs. (34) and (36). However, in this case the main component of the SDM (fragmented in the TBA without projection) gives the large background in the strength function if the smearing parameter Δ in Eq. (7) is not very small. The calculations for ^{48}Ca were performed with $\Delta = 100$ keV, and to remove this background the contribution of the main component of the SDM into the strength functions was eliminated with the help of subtraction of the SDM term with the minimum energy from the polarizability (8). The difference δCTBA(Q^{bare}) between the functions $F(E)$ calculated within the CTBA+ and CTBA for the bare IS $E1$ operator is shown in Fig. 5 by the black full line. As can be seen, the absolute values of δCTBA(Q^{bare}) are on average much larger than the values of the analogous difference δCTBA(Q^{eff}) calculated

TABLE I. Integral characteristics of the differences of the strength distributions shown in Fig. 5. The relative mean-square deviation $||\delta S||_{\text{R}}$ is determined by Eqs. (77)–(79).

Interval (MeV)	$||\delta S||_{\text{R}}$		
	δCTBA(Q^{bare})	δCTBA(Q^{eff})	δCTBA+
5–25	0.43	0.008	0.05
0–60	0.31	0.006	0.04

for the effective IS $E1$ operator, which are shown in Fig. 5 by the red dotted line. On the other hand, the difference δCTBA+ between the CTBA+ results obtained for the IS $E1$ operators Q^{bare} and Q^{eff} (shown by the green dashed line) is small.

Differences of the strength distributions shown in Fig. 5 can be quantified with the help of the following relative mean-square deviation:

$$||\delta S||_{\text{R}} = ||\delta S||/||S||, \tag{77}$$

with

$$||\delta S||^2 = \int_{E_1}^{E_2} (\tilde{S}(E) - S(E))^2 dE, \tag{78}$$

$$||S||^2 = \int_{E_1}^{E_2} S^2(E)\, dE, \tag{79}$$

where $S(E)$ is the strength function calculated within the CTBA+ (for the IS $E1$ operator Q^{eff} in the case of δCTBA+) and $\tilde{S}(E)$ is the strength function calculated within the versions of the CTBA and CTBA+ shown in Fig. 5.

For the energy intervals 5–25 and 0–60 MeV in Eqs. (78) and (79), the values of $||\delta S||_{\text{R}}$ are listed in Table I. The large values of $||\delta S||_{\text{R}}$ for the difference δCTBA(Q^{bare}) show that the coupling of the SDM with physical modes in the CTBA response function for the IS $E1$ excitations is quite appreciable. However, the small values of $||\delta S||_{\text{R}}$ for δCTBA(Q^{eff}) and δCTBA+ suggest, first, that this coupling is effectively eliminated in the CTBA+ response function and, second, that the strength of the SDM fragments resulting from this coupling in the excitation spectrum of the CTBA is strongly suppressed by the effective IS $E1$ operator Q^{eff}, as mentioned above.

In Fig. 6, the results for the GDR in ^{48}Ca and ^{48}Ni are shown. The $E1$ photoabsorption cross section shown in this figure is connected with the strength function (7) for the effective isovector $E1$ operator, Eqs. (37) and (40), by means of the known formula (see, e.g., [36]). The strength functions for this operator were calculated with the smearing parameter $\Delta = 500$ keV. The curve denoted as $100\times\delta$CTBA corresponds here to the difference between the cross sections calculated within the CTBA+ and CTBA multiplied by the factor of 100. As in the case of the IS $E1$ excitations, this difference is very small. It vanishes below 10 MeV, where the isovector $E1$ strength in ^{48}Ca and ^{48}Ni is absent.

The agreement between the theory and experiment in ^{48}Ca is noticeably improved in the CTBA as compared to the CRPA. The form of the experimental $E1$ photoabsorption cross section is on the whole reproduced in the CTBA, though
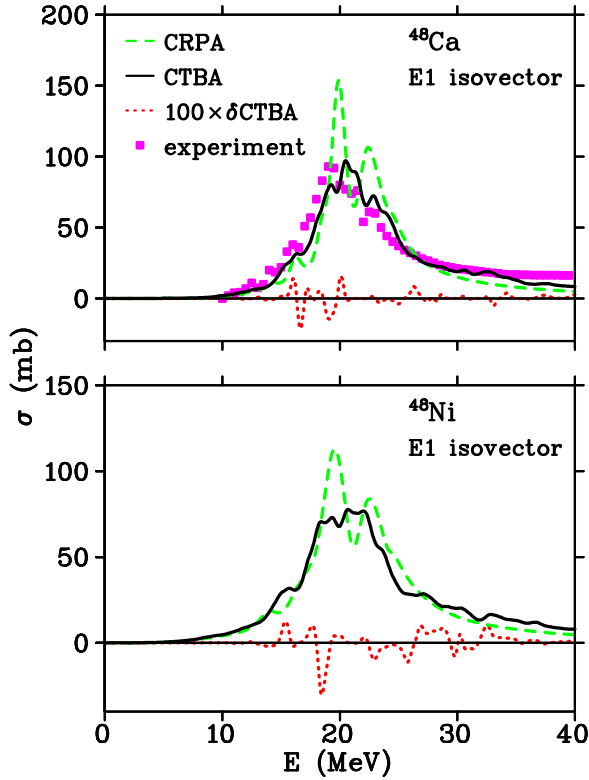
FIG. 6. Upper panel: the $E1$ photoabsorption cross section for ^{48}Ca calculated within the CRPA (green dashed line) and CTBA (black full line) based on the Skyrme-EDF parametrization SV-m64k6. The red dotted line represents the difference δCTBA between the CTBA+ and CTBA results multiplied by the factor of 100. The smearing parameter $\Delta = 500$ keV was used in the calculations of the strength functions. Experimental data from Ref. [52] are represented by magenta squares. Lower panel: same as in the upper panel but for ^{48}Ni.

the position of the main peak in the CTBA is shifted upward by about 1.3 MeV with respect to the experiment.

2. Pygmy dipole resonance in ^{208}Pb

Calculations of the pygmy dipole resonance (PDR) in ^{208}Pb were performed with the use of the Skyrme-EDF parametrization SKXm$_{-0.49}$ from Ref. [47]. The spin-orbit and spin-spin parameters of SKXm$_{-0.49}$ were fitted with the aim of describing the $M1$ resonance in ^{208}Pb within the RenTBA. The other parameters coincide with parameters of the original Skyrme interaction SKXm [53]. In the present paper, as mentioned above, a modified version of the renormalization scheme of the RenTBA is used. In this case the results of Ref. [47] for the $M1$ resonance in ^{208}Pb are reproduced at the slight change of the spin-spin Landau-Migdal parameters g and g'. Note that these parameters do not affect the ground-state properties of the even-even spherical nuclei. In the calculations presented below the values $g = 0.086$ and $g' = 0.87$ are used (the other parameters of SKXm$_{-0.49}$ are the same as in Ref. [47]). The box radius in ^{208}Pb was equal to 18 fm and the parameter $\varepsilon_{max} = 100$ MeV. It gives $\omega_{SDM} = 0.78$ MeV. The resulting phonon space of the RenTBA included 124 phonons of
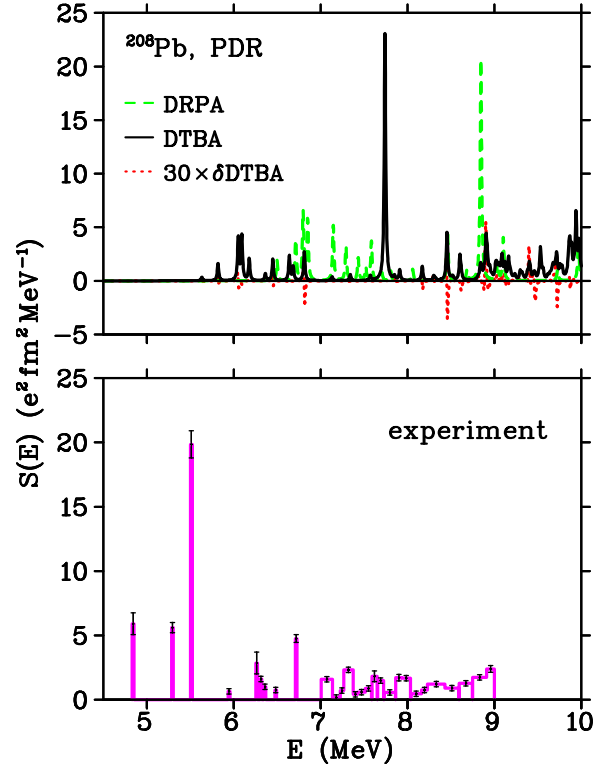
FIG. 7. Upper panel: pygmy dipole resonance in ^{208}Pb calculated within the DRPA (green dashed line) and DTBA (black full line) based on the Skyrme-EDF parametrization SKXm$_{-0.49}$. The red dotted line represents the difference δDTBA between the DTBA+ and DTBA results multiplied by the factor of 30. The smearing parameter $\Delta = 10$ keV was used. Lower panel: experimental $E1$ strength distribution in ^{208}Pb from Ref. [54]. See text for more details.

electric type with multipolarities $1 \leqslant L \leqslant 12$ and 73 phonons of magnetic type with multipolarities $0 \leqslant L \leqslant 14$. All the obtained phonons' energies are less than 11 MeV.

On the upper panel of Fig. 7, the strength distributions of the PDR in ^{208}Pb calculated within the fully self-consistent DRPA and DTBA are shown. The single-particle continuum was not included because it plays a minor role here. The strength functions for the effective isovector $E1$ operator determined by Eqs. (37) and (40) have been calculated with the small smearing parameter $\Delta = 10$ keV to expose the fine structure of the PDR. The curve denoted as $30 \times \delta$DTBA corresponds to the difference between the functions $S(E)$ calculated within the DTBA+ and DTBA multiplied by the factor of 30. This difference is small as in the cases of calculations for ^{48}Ca and ^{48}Ni discussed above.

The experimental data from Ref. [54] are presented in the lower panel of Fig. 7 in the form of the distribution of the summed $B(E1)$ strengths in the energy bins divided by the width of the bin ΔE. Such a distribution corresponds to the strength function $S(E)$ with the energy-dependent smearing parameter Δ. For the isolated 1^- states below 7 MeV, the value of ΔE was taken to be 20 keV in accordance with the value of the smearing parameter in the DRPA and DTBA calculations.
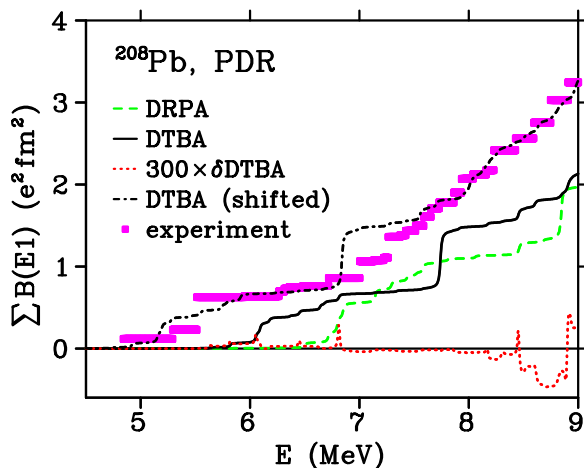
FIG. 8. Summed strength of the $E1$ excitations in ^{208}Pb in the region of the pygmy dipole resonance calculated within the DRPA (green dashed line) and DTBA (black full line) based on the Skyrme-EDF parametrization SKX$m_{-0.49}$. The red dotted line represents the difference δDTBA between the DTBA+ and DTBA results multiplied by the factor of 300. The black dash-dotted line represents the DTBA result shifted down by 0.9 MeV. The experimental data from Ref. [54] are represented by magenta squares.

As was noted in Ref. [55], the PDR in ^{208}Pb can be divided into two parts: a lower one from 4.8 to about 5.7 MeV and an upper one from 5.7 to 8.23 MeV. At higher energies, according to analysis of Ref. [54], the distribution of the $E1$ strength corresponds to the low-energy tail of the GDR. However, the $E1$ strength below 5.7 MeV is absent both in the DRPA and in the DTBA distributions shown in Fig. 7. In general, it is a problem of many self-consistent calculations of the PDR in ^{208}Pb; see [55] for a more detailed discussion. Although a comparison of the theory with the experimental data is not the aim of the present paper, consider how the situation looks for the summed $E1$ strength in ^{208}Pb in the PDR region. The respective results are shown in Fig. 8. First, one can see that the difference between the DTBA+ and DTBA results for the summed $E1$ strength is practically absent below 8 MeV and is negligibly small in the interval 8–9 MeV. Second, the DTBA curve fairly well reproduces the data (except for the region around 7 MeV) *if* this curve is shifted down by 0.9 MeV. The DTBA itself gives a downward shift of the $E1$ strength

as compared to the DRPA but this shift is insufficient. One of the possible ways to diminish this discrepancy between the theory and experiment is generalization of the RenTBA including so-called ground-state correlations beyond the RPA (see Refs. [56,57] for more details).

V. CONCLUSIONS

In this work, the range of the problems related to the existence of the spurious dipole mode (SDM) in self-consistent nuclear-structure models is considered.

An explicit form of the SDM terms of the RPA response function was derived from the symmetry properties of the underlying energy-density functional. This form was used to construct the projection operator P which enables one (i) to eliminate the SDM contributions from the RPA response function and (ii) to eliminate coupling of the SDM with the physical modes in the extended RPA (ERPA) theories. The equation for the response function in the ERPA with projection (ERPA+, in which the above-mentioned coupling is eliminated) is formulated. It is shown that the action of the operator P on the bare external-field $E1$ operators yields the well-known isoscalar and isovector effective $E1$ operators.

Numerical examples of the application of the projection method are considered. As the model of the ERPA type, the time blocking approximation (TBA) is used. It is shown that the TBA+ version of the model is quite efficient for eliminating the coupling of the SDM with the physical modes. However, the difference between the results of the realistic calculations of the $E1$ excitations within the TBA and TBA+ is very small if the effective external-field $E1$ operators are used. The reason is that the strength of the SDM fragments in the TBA response function is strongly suppressed by the effective operators. At the same time, the difference between the TBA and TBA+ results becomes appreciable in the case of the bare $E1$ operators.

ACKNOWLEDGMENTS

[1] H. J. Mikeska and W. Brenig, Z. Phys. **220**, 321 (1969).

[2] J. Speth, E. Werner, and W. Wild, Phys. Rep. **33**, 127 (1977).

[3] V. A. Khodel and E. E. Saperstein, Phys. Rep. **92**, 183 (1982).

[4] P. Ring and P. Schuck, *The Nuclear Many-Body Problem* (Springer-Verlag, New York, 1980).

[5] J.-P. Blaizot and G. Ripka, *Quantum Theory of Finite Systems* (MIT Press, Cambridge, MA, 1986).

[6] M. Bender, P.-H. Heenen, and P.-G. Reinhard, Rev. Mod. Phys. **75**, 121 (2003).

[7] J. E. Drut, R. J. Furnstahl, and L. Platter, Prog. Part. Nucl. Phys. **64**, 120 (2010).

[8] M. Grasso, Prog. Part. Nucl. Phys. **106**, 256 (2019).

[9] J. P. Elliott and T. H. R. Skyrme, Proc. R. Soc. London A **232**, 561 (1955).

[10] S. Gartenhaus and C. Schwartz, Phys. Rev. **108**, 482 (1957).

[11] H. J. Lipkin, Phys. Rev. **110**, 1395 (1958).

[12] E. Caurier, G. Martínez-Pinedo, F. Nowacki, A. Poves, and A. P. Zuker, Rev. Mod. Phys. **77**, 427 (2005).

[13] G. Hagen, T. Papenbrock, and D. J. Dean, Phys. Rev. Lett. **103**, 062503 (2009).

[14] B. R. Barrett, P. Navrátil, and J. P. Vary, Prog. Part. Nucl. Phys. **69**, 131 (2013).

[15] H. Hergert, S. K. Bogner, T. D. Morris, A. Schwenk, and K. Tsukiyama, Phys. Rep. **621**, 165 (2016).

[16] G. De Gregorio, F. Knapp, N. Lo Iudice, and P. Veselý, Phys. Lett. B **821**, 136636 (2021).

[17] G. De Gregorio, F. Knapp, N. Lo Iudice, and P. Veselý, Phys. Rev. C **105**, 024326 (2022).

[18] A. M. Lane and J. Martorell, Ann. Phys. (NY) **129**, 273 (1980).

[19] T. Nakatsukasa, T. Inakura, and K. Yabana, Phys. Rev. C **76**, 024318 (2007).

[20] A. Repko, J. Kvasil, and V. O. Nesterenko, Phys. Rev. C **99**, 044307 (2019).

[21] J. Kvasil, A. Repko, and V. O. Nesterenko, Eur. Phys. J. A **55**, 213 (2019).

[22] M. Tohyama and P. Schuck, Eur. Phys. J. A **19**, 203 (2004).

[23] M. Tohyama and P. Schuck, Eur. Phys. J. A **32**, 139 (2007).

[24] D. Gambacurta, M. Grasso, and F. Catara, Phys. Rev. C **81**, 054312 (2010).

[25] D. Gambacurta, M. Grasso, and F. Catara, Phys. Rev. C **84**, 034301 (2011).

[26] K. Mizuyama and G. Colò, Phys. Rev. C **85**, 024307 (2012).

[27] V. I. Tselyaev, Phys. Rev. C **88**, 054301 (2013).

[28] V. I. Tselyaev, in *II Russian-Spanish Congress on Particle and Nuclear Physics at All Scales, Astroparticle Physics and Cosmology, 1–4 October 2013, St. Petersburg, Russia*, edited by A. Andrianov, D. Espriu, V. Andrianov, and S. Kolevatov, AIP Conf. Proc. No. 1606 (AIP, New York, 2014), p. 201.

[29] V. I. Tselyaev, Phys. At. Nucl. **61**, 739 (1998).

[30] N. Van Giai and H. Sagawa, Nucl. Phys. A **371**, 1 (1981).

[31] N. I. Pyatov and D. I. Salamov, Nukleonika **22**, 127 (1977).

[32] E. Tabar, H. Yakut, A. A. Kuliev, G. Hoşgör, E. Kemah, and H. Quliyev, Nucl. Phys. A **1001**, 121885 (2020).

[33] A. B. Migdal, *Theory of Finite Fermi Systems and Application to Atomic Nuclei* (Wiley, New York, 1967).

[34] R. Ring, P. Bauer and J. Speth, Nucl. Phys. A **206**, 97 (1973).

[35] V. Tselyaev, N. Lyutorovich, J. Speth, G. Martinez-Pinedo, K. Langanke, and P.-G. Reinhard, arXiv:2201.08838.

[36] E. V. Litvinova and V. I. Tselyaev, Phys. Rev. C **75**, 054318 (2007).

[37] N. Lyutorovich, V. Tselyaev, J. Speth, S. Krewald, F. Grümmer, and P.-G. Reinhard, Phys. Lett. B **749**, 292 (2015).

[38] N. Lyutorovich, V. Tselyaev, J. Speth, S. Krewald, and P.-G. Reinhard, Phys. At. Nucl. **79**, 868 (2016).

[39] V. Tselyaev, N. Lyutorovich, J. Speth, S. Krewald, and P.-G. Reinhard, Phys. Rev. C **94**, 034306 (2016).

[40] Y. F. Niu, G. Colò, E. Vigezzi, C. L. Bai, and H. Sagawa, Phys. Rev. C **94**, 064328 (2016).

[41] X. Roca-Maza, Y. F. Niu, G. Colò, and P. F. Bortignon, J. Phys. G: Nucl. Part. Phys. **44**, 044001 (2017).

[42] D. Gambacurta, M. Grasso, and J. Engel, Phys. Rev. C **92**, 034303 (2015).

[43] D. Gambacurta and M. Grasso, Eur. Phys. J. A **52**, 198 (2016).

[44] V. I. Tselyaev, Phys. Rev. C **75**, 024306 (2007).

[45] E. Chabanat, P. Bonche, P. Haensel, J. Meyer, and R. Schaeffer, Nucl. Phys. A **635**, 231 (1998).

[46] V. Tselyaev, N. Lyutorovich, J. Speth, and P.-G. Reinhard, Phys. Rev. C **97**, 044308 (2018).

[47] V. Tselyaev, N. Lyutorovich, J. Speth, and P.-G. Reinhard, Phys. Rev. C **102**, 064319 (2020).

[48] N. Lyutorovich, V. I. Tselyaev, J. Speth, S. Krewald, F. Grümmer, and P.-G. Reinhard, Phys. Rev. Lett. **109**, 092502 (2012).

[49] V. Tselyaev, N. Lyutorovich, J. Speth, P.-G. Reinhard, and D. Smirnov, Phys. Rev. C **99**, 064329 (2019).

[50] Y.-W. Lui, D. H. Youngblood, S. Shlomo, X. Chen, Y. Tokimoto, Krishichayan, M. Anders, and J. Button, Phys. Rev. C **83**, 044327 (2011).

[51] M. R. Anders, S. Shlomo, T. Sil, D. H. Youngblood, Y.-W. Lui, and Krishichayan, Phys. Rev. C **87**, 024303 (2013).

[52] V. A. Erokhova, M. A. Elkin, A. V. Izotova, B. S. Ishkhanov, I. M. Kapitonov, E. I. Lileeva, and E. V. Shirokov, Bull. Russ. Acad. Sci. Phys. **67**, 1636 (2003).

[53] B. A. Brown, Phys. Rev. C **58**, 220 (1998).

[54] I. Poltoratska, P. von Neumann-Cosel, A. Tamii, T. Adachi, C. A. Bertulani, J. Carter, M. Dozono, H. Fujita, K. Fujita, Y. Fujita, K. Hatanaka, M. Itoh, T. Kawabata, Y. Kalmykov, A. M. Krumbholz, E. Litvinova, H. Matsubara, K. Nakanishi, R. Neveling, H. Okamura *et al.*, Phys. Rev. C **85**, 041304(R) (2012).

[55] N. A. Lyutorovich, V. I. Tselyaev, O. I. Achakovskiy, and S. P. Kamerdzhiev, JETP Lett. **107**, 659 (2018).

[56] S. P. Kamerdzhiev, G. Y. Tertychnyǐ, and V. I. Tselyaev, Phys. Part. Nuclei **28**, 134 (1997).

[57] S. Kamerdzhiev, J. Speth, and G. Tertychny, Phys. Rep. **393**, 1 (2004).